J Mater Sci: Mater Electron (2022) 33:3738–3747

The crystal structure, sintering behavior and microwave dielectric properties of $BiZn_2PO_6$ ceramics for ULTCC applications

Ping Zhang[1,*], Xin Tian[1], Manman Hao[1], and Sheng Xie[1,*]

[1] *School of Electrical and Information Engineering, School of Microelectronics and Key Laboratory of Advanced Ceramics and Machining Technology of Ministry of Education, Tianjin University, Tianjin 300072, People's Republic of China*

Received: 31 July 2021
Accepted: 9 December 2021
Published online: 5 February 2022

ABSTRACT

A novel $BiZn_2PO_6$ ceramic with good performance was composited under ultra-low-temperature through the traditional solid-state reaction method. The crystal structure, microstructure and microwave dielectric properties of $BiZn_2PO_6$ ceramics were analyzed in detail. The XRD spectra showed that the pure crystal phase of $BiZn_2PO_6$ ceramic was obtained successfully. The results of further Rietveld refinement based on XRD data indicated that $BiZn_2PO_6$ ceramic possessed an orthorhombic structure. The density of $BiZn_2PO_6$ ceramics was reflected by SEM micrographs, grain size distribution and relative density data. The relative density of $BiZn_2PO_6$ ceramic sintered at 725 °C for 4 h reached 97.8%. The pure $BiZn_2PO_6$ ceramic sintered at 725 °C had the best properties, the data of permittivity, quality factor and resonant frequency temperature coefficient were as follows: ε_r = 13.269, $Q \times f$ = 18,030 GHz, τ_f = − 18.9 ppm/°C.

1 Introduction

Thanks to the continuous advancement of modern information technology, especially communication technology, we ushered in a new era of 5G. The 5th generation mobile communication uses many key technologies, among which millimeter wave technology can achieve ultra-high speed wireless data transmission by increasing spectrum bandwidth. In this context, it is evident that microwave dielectric ceramic materials have ushered in a broad application prospect due to their unique advantages [1–5]. On the one hand, low permittivity materials can reduce the delay of high-frequency electrical signal transmission and can be used as substrates. On the other hand, materials with resonant frequency temperature coefficient close to zero could ensure thermal stability, and a high-quality factor means low dielectric loss [6, 7]. Therefore, they are now commonly used in many fields of microwave technology, such as mobile phones, satellite broadcasting, radar and navigation. [8]. They are used to make resonators, stabilized oscillator filters, dielectric substrates, discriminators, dielectric antennas, etc. It is

Address correspondence to E-mail: zhangping@tju.edu.cn; xie_sheng06@tju.edu.cn

https://doi.org/10.1007/s10854-021-07565-z

worth noting that the sintering temperature of microwave dielectric ceramics is an important influencing factor. The technology of low-temperature co-fired ceramics (LTCC) has attracted the interest of many scholars and has been extensively studied in recent years, which has been proven that it has a great potential for miniaturization and integration of microwave components [9–11]. In addition, ULTCC has become one of the hot spots in the field of functional materials in recent years due to its advantages over LTCC in some aspects [12, 13]. As the main dielectric material for passive integration technology, ultra-low-temperature sintered microwave dielectric ceramics have important application value and theoretical guidance. For example, in this technology, low-cost aluminum is expected to replace silver electrodes as the electrode material, while the ultra-low sintering temperature will also effectively reduce energy consumption and prevent reactions with other materials [14].

Most of the microwave dielectric ceramics with low dielectric loss that have been reported so far are sintered at high temperatures. Adding low melting point oxides such as TeO_2, Bi_2O_3 and Li_2O is usually a conventional method to reduce the sintering temperature of ceramics. Nevertheless, it often brings some negative effects simultaneously, such as deterioration of properties and reduction of mechanical strength. Some scholars have noted the advantages of phosphate ceramics, such as typically sintered at low-temperatures and having low dielectric constants. Meanwhile, some phosphate ceramics with olivine structure also combine excellent microwave dielectric properties with good electrode compatibility, so they are gradually discovered and reported [15, 16]. Chen et al. [17] completed the preparation of Li_2CO_3, ZnO and $NH_4H_2PO_4$ according to the stoichiometric ratio, and then sintered $LiZnPO_4$(LZP) ceramics by solid-state reaction at 825 °C with their performance analyzed as well. The result shows that $\varepsilon_r = 5.3$, $Q \times f = 28496$ GHz, and $\tau_f = -80.4$ ppm/°C, which means that LZP ceramics have good properties. Further, the negative resonant frequency can be facilely tuned to near zero by adding TiO_2.

Subsequently, several scholars have followed up on the lattice structure and dielectric properties and their relationships, such as the substitution of divalent ions (Ni^{2+}, Co^{2+}, Mn^{2+}) at the Zn-site [18–20]. It was demonstrated that the cation substitution led to changes in the tetrahedral bond length and electron density distribution of ZnO_4, and the microwave dielectric properties were significantly improved. There are relatively few reports on $BiZn_2PO_6$, and the available reports have focused on crystallographic, magnetic, or thermal properties [21, 22]. In their work, they systematically the elastic anisotropy and thermodynamics of $BiZn_2PO_6$ using first-principles methods. They pointed out that the orthogonal $BiZn_2PO_6$ ceramic is structurally stable and has high mechanical strength. So far, no statements about crystal structure, microstructure, relative densities, and dielectric properties of $BiZn_2PO_6$ have been reported.

In this paper, we did the above work and analyzed the results in detail for the first time. We found that $BiZn_2PO_6$ ceramics could be sintered at ultra-low-temperatures and exhibit excellent performance.

As mentioned above, ULTCC is a key technology with great potential, but the development of ULTCC is still in its infancy. There are few reports of materials that meet the requirements for ULTCC applications. Some scholars pay attention to tungstates and vanadates. Most of them have low loss, but only a small part of new tungsten-based and vanadium-based ceramic materials are suitable for ultra-low-temperature sintering ceramic materials [23, 24]. Other scholars have focused on tellurates. Most tellurates have ultra-low sintering temperatures and good properties, but they are toxic and expensive [25, 26]. Besides, glass has a lower softening temperature, the sintering temperature of glass–ceramic can be lower than 700 °C, so some researchers have done ultra-low-temperature research from this perspective [27, 28]. However, glass–ceramic absorbs energy at high frequencies, resulting in a low $Q \times f$ value [13].

In summary, few ceramic materials suitable for ULTCC have been developed and reported. The novel ceramic of $BiZn_2PO_6$ in our work has the advantages of low permittivity, high $Q \times f$ values, ultra-low sintered temperature, and low price. It is suitable for the growing demand for ULTCC applications.

2 Experimental procedures

According to the stoichiometric ratio, analytical grade powders of Bi_2O_3, $NH_4H_2PO_4$, ZnO were used to compose $BiZn_2PO_6$ ceramic by traditional solid-state

reaction. First, the raw material and appropriate deionized water were placed in a jar filled with zirconia. Then, the mixture was ball-grinded on a ball mill for 4 h, the purpose of primary ball milling was to initially improve the particle size of raw materials and to mix raw materials fully. The slurry mixture after dried and sieved was calcined in an alumina crucible at 600 °C. Then deionized water was added to the obtained $BiZn_2PO_6$ powders and it was ground again for another 4 h. The purpose of the second ball milling is to further granulate the calcined powder and to enhance the activity of the powder. The slurry obtained in the previous step was dried, screened and ground into a powder. And then, 8% paraffin was added as a binder and the mixture was finally pressed into a small cylinder under the pressure of 4 MPa. The radius and height of the small cylinders were 5 mm. Afterward, the cylinders were sintered at 550 °C for 2 h to expel the binder. Then, the furnace was adjusted to increase the temperature at a rate of three degrees per minute until the cylinders were sintered. The sintering temperature in this experiment is from 675 to 775 °C, which is a relatively low-temperature range.

The crystalline phases of the sintered samples were reviewed by X-diffraction (XRD, Rigaku D/max 2550 PC, Tokyo, Japan) with Cu Kα radiation (V = 200 kV, I = 40 mA) over the 2θ range of 10°–70°. The processing and analysis of the XRD pattern were done with jade software, and further refined by FullProf_suite. The TE01δ shielded cavity method was used to measure the microwave dielectric properties of the samples with a network analyzer (N5234A, Agilent Co., America) in the frequency range of 7–13 GHz. The temperature coefficient of the resonant frequency could be calculated by Eq. (1), where the temperature range is 25–85 °C:

$$\tau_f = \frac{f_2 - f_1}{f_1(T_2 - T_1)} \times 10^6 (\mathrm{ppm}/^{\circ}\mathrm{C}) \quad (1)$$

Among them, f_1 and f_2 are the corresponding frequencies when the temperature at temperatures T_1 and T_2, respectively. The bulk density of $BiZn_2PO_6$ ceramics was measured by the Archimedes method. And the theoretical density was calculated by Eq. (2):

$$\rho_{\mathrm{theory}} = \frac{ZA}{V_c N_A} \quad (2)$$

In this equation, Z, A, V_C, and N_A represent the number of atoms per unit cell, the atomic molar mass, the volume per unit cell, and the Avogadro constant in turn. According to the bulk densities and theoretical densities obtained in the experiment, the relative densities at different temperatures can be calculated through Eq. (3):

$$\rho_{\mathrm{relative}} = \frac{\rho_{\mathrm{bulk}}}{\rho_{\mathrm{theory}}} \times 100\% \quad (3)$$

3 Results and discussion

Figure 1 displays the XRD spectra of the sample of $BiZn_2PO_6$ ceramic which was sintered at 725 °C. According to the standard card (ICSD-91234) of $BiZn_2PO_6$ belonging to the orthorhombic, all peaks in the spectrum formed by X-ray diffraction could be matched. The absence of other peaks in the plot indicates that no other unknown phases can be found in the $BiZn_2PO_6$ ceramics.

Figure 2 displays the Rietveld refinement of $BiZn_2PO_6$ ceramic based on the XRD pattern mentioned above. The blue line shows the difference between the calculated and observed intensities, and the green line shows the position of the Bragg reflection. The structure refinement data, including unit cell parameters, chemical bond types and bond lengths, and atomic position information, were put in Table 1, Table 2, and Table 3, respectively. Among them, Table 1 shows some information about the unit cell parameters, including the lattice parameters and the unit cell volume (V_{unit}) of the $BiZn_2PO_6$ ceramic. The lattice parameters are a = 11.8941 Å, b = 5.2754 Å, c = 7.8162 Å. The theoretical density of

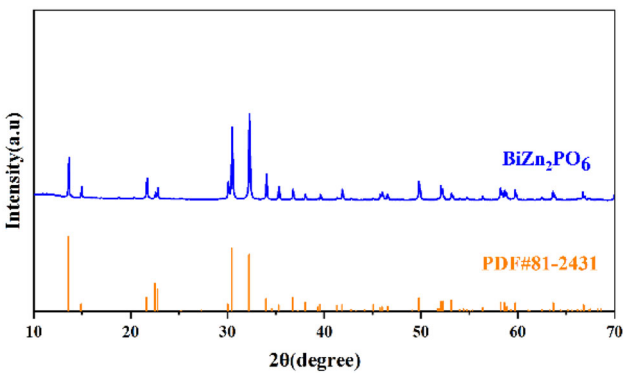

Fig. 1 The X-ray diffraction pattern of $BiZn_2PO_6$ ceramic sintered at 725 °C for 4 h

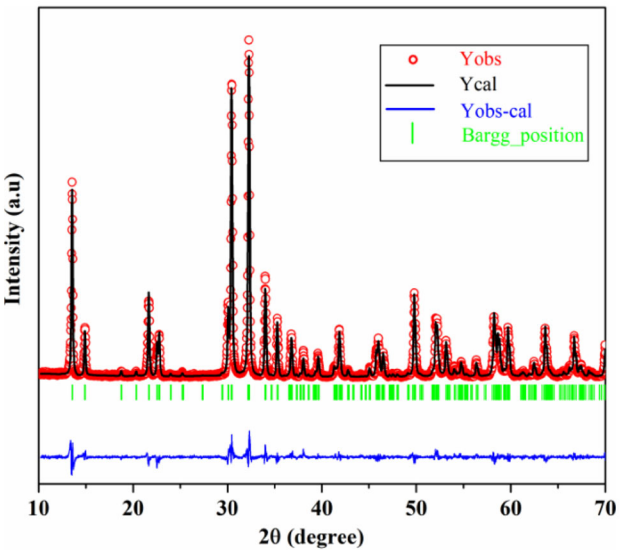

Fig. 2 Refinement result of $BiZn_2PO_6$ ceramic sintered at 725 °C for 4 h

$BiZn_2PO_6$ ceramic is 6.32 g/cm^3, which can be calculated from cell volume and relative atomic mass. The reliability factor of patterns (R_p) and the reliability factor of weighted patterns (R_{wp}) ranged from 13.3 to 14.7, indicating that the refining results are excellent.

Figure 3a shows the crystal structure of $BiZn_2PO_6$. The Bi atom is attached to four O(1) atoms in the form of covalent bonds to form a BiO_4 square pyramid. And each O(1) atom is connected to two Bi atoms, creating a zigzag chain. The PO_4^{3-} groups are distorted with two short distances with O(3) and O(4) atoms which shared with $Zn(2)O_5$ and $Zn(1)O_5$ polyhedron, respectively, while two longer distances with O(2) atoms are involved in the coordination of both Zn(1) and Zn(2) atoms. Zn^{2+} cations are located in the center of the Zn(1) or Zn(2) tetrahedron, which consists of two O(1), two O(2), and one O(3) or one O(4) atom, respectively. Moreover, PO_4 tetrahedra are independent while PO_4^{3-} corner connected with ZnO_5 square pyramids [29]. The three-dimensional framework of $BiZn_2PO_6$ belongs to the orthorhombic system. Figure 3(b) shows a detailed view of polyhedrons with different structures.

Figure 4 shows the surface SEM micrographs of $BiZn_2PO_6$ ceramics sintered at different temperatures, and the grain size distribution of the corresponding samples are inserted in the lower right corner, respectively. When the sintering temperature is 675 °C, there are many pores on the surface of the ceramic, resulting in relatively low density. When the sintering temperature rises to 700 °C, the number of pores decreases significantly and the average grain

Table 1 Reliability factors, lattice parameters, and V_{unit} of $BiZn_2PO_6$ ceramics at 725 °C

Component	Reliability factors		Lattice parameters			V_{unit} (Å^3)
	R_p (%)	R_{wp} (%)	a (Å)	b (Å)	c (Å)	
$BiZn_2PO_6$	13.3	14.7	11.8941	5.2754	7.8162	490.43

Table 2 The bond type, bond length, lattice energy of $BiZn_2PO_6$ ceramics after refinement

Atom	Bond type	Bond length (Å)	Lattice energy (KJ/mol)	Average (KJ/mol)
Bi	Bi–O(1)^1	2.34 × 2	2028	1862.5
	Bi–O(1)^2	2.301 × 2	2055	
	Bi–O(3)	3.063 × 2	1645	
	Bi–O(4)	2.94 × 1	1722	
Zn(1)	Zn(1)–O(1)	1.97 × 2	1537	1478.7
	Zn(1)–O(2)	2.084 × 2	1467	
	Zn(1)–O(4)	2.05 × 1	1432	
Zn(2)	Zn(2)–O(1)	1.97 × 2	1537	1490
	Zn(2)–O(2)	2.016 × 2	1505	
	Zn(2)–O(3)	2.116 × 1	1428	
P	P–O(2)	1.557 × 2	5189	6106.3
	P–O(3)	1.443 × 1	6296	
	P–O(4)	1.43 × 1	6834	

Table 3 Wyckoff position of $BiZn_2PO_6$ ceramics after refined

Element	Wyckoff position	*x*	*y*	*z*
Bi	4c	0.0990 (2)	0.25	0.0119 (3)
Zn(1)	4c	0.1028 (7)	0.75	0.6915 (6)
Zn(2)	4c	0.0930 (7)	0.75	0.3011 (6)
P	4c	0.1945 (8)	0.25	0.481 (2)
O(1)	8d	− 0.010 (2)	− 0.006 (4)	0.191 (2)
O(2)	8d	0.123 (1)	0.497 (1)	0.489 (3)
O(3)	4c	0.285 (1)	0.25	0.604 (2)
O(4)	4c	0.245 (2)	0.25	0.315 (3)

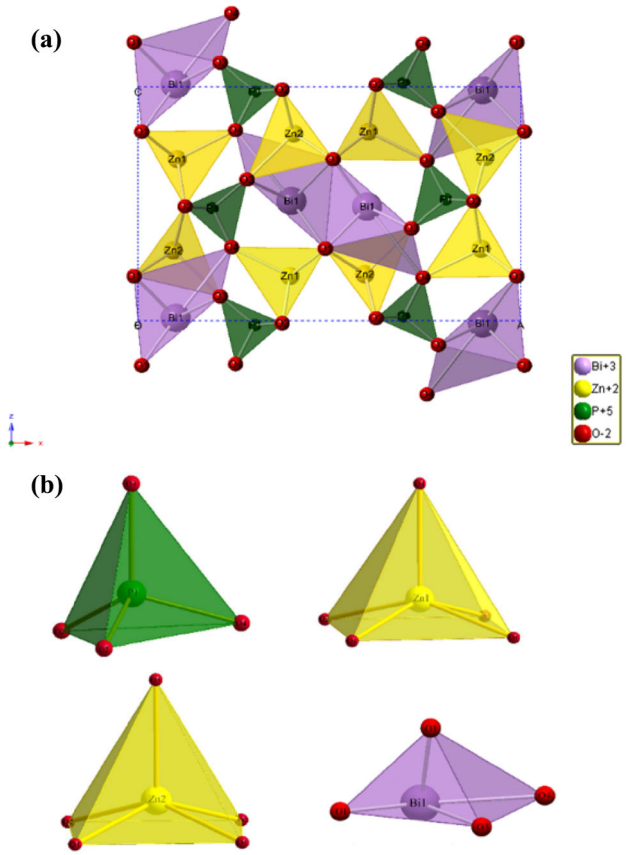

Fig. 3 **a** The crystal structure of $BiZn_2PO_6$ ceramic. **b** A detailed view of polyhedrons with different structures

size increases. When reaching 725 °C, the density was best with clear grain boundaries and relatively uniform grain size, reaching an average size of 1.24 μm. However, the average grain size decreased to 1.17 μm when the temperature was increased to 750 °C. When sintered at 775 °C, some grains started to melt, indicating that the sintering temperature was too high.

Figure 5 shows properties of $BiZn_2PO_6$ ceramics sintered at different temperatures, including the relative density, permittivity, and $Q \times f$ values. The relative density of each sintered sample increases first and reaches the maximum at 725 °C. And then, the relative density decreases with the gradual increase of sintering temperature. Moreover, it can be seen from the figure that all relative density data reach 90%. We have compiled the relevant reports for BiM_2AO_6 (M = Cu, Mg, Ca, Mn, Pb; A = As, V, P) systems with similar structures, as shown in Table 4 [30–32]. The comparison results show that the density data obtained for the present work at different temperatures are ideal. Under the condition of sintered at the optimum sintered temperature, the bulk density of $BiZn_2PO_6$ is 6.18 g/cm^3, and the theoretical density mentioned above is 6.32 g/cm^3. The calculated relative density reaches 97.8%, which shows that we have obtained novel ceramics with the highest density when sintered at 725 °C. The variation trend of the permittivity and the $Q \times f$ value keeps consistent with the variation law of the relative density. We noticed that the ε_r value increased gradually in the range of 675–725 °C and reached maximum values of 13.269 at 725 °C. The value of permittivity is mainly related to the density, cell volume, ion polarizability, and the presence of impurities [33]. In this paper, according to the XRD pattern results above, no second phase is generated, so the ε_r value is primarily determined by the ionic polarizability and the relative density. As for theoretical ion polarizability, expressed here by α_{theo}, can be obtained by Eq. (4). The theoretical basis of this formula is Shannon's additive rule [34].

$$\alpha_{\text{theo}} = \alpha_{Bi^{3+}} + 2\alpha_{Zn^{2+}} + \alpha_{P^{5+}} + 6\alpha_{O^{2-}} \quad (4)$$

Furthermore, from Shannon's research, we can get the values in the above formula, where $\alpha(Bi^{3+})$ = 6.12 Å^3, $\alpha(Zn^{2+})$ = 2.04 Å^3, $\alpha(P^{5+})$ = 1.22 Å^3, and $\alpha(O^{2-})$ = 2.01 Å^3. Then, we can calculate the

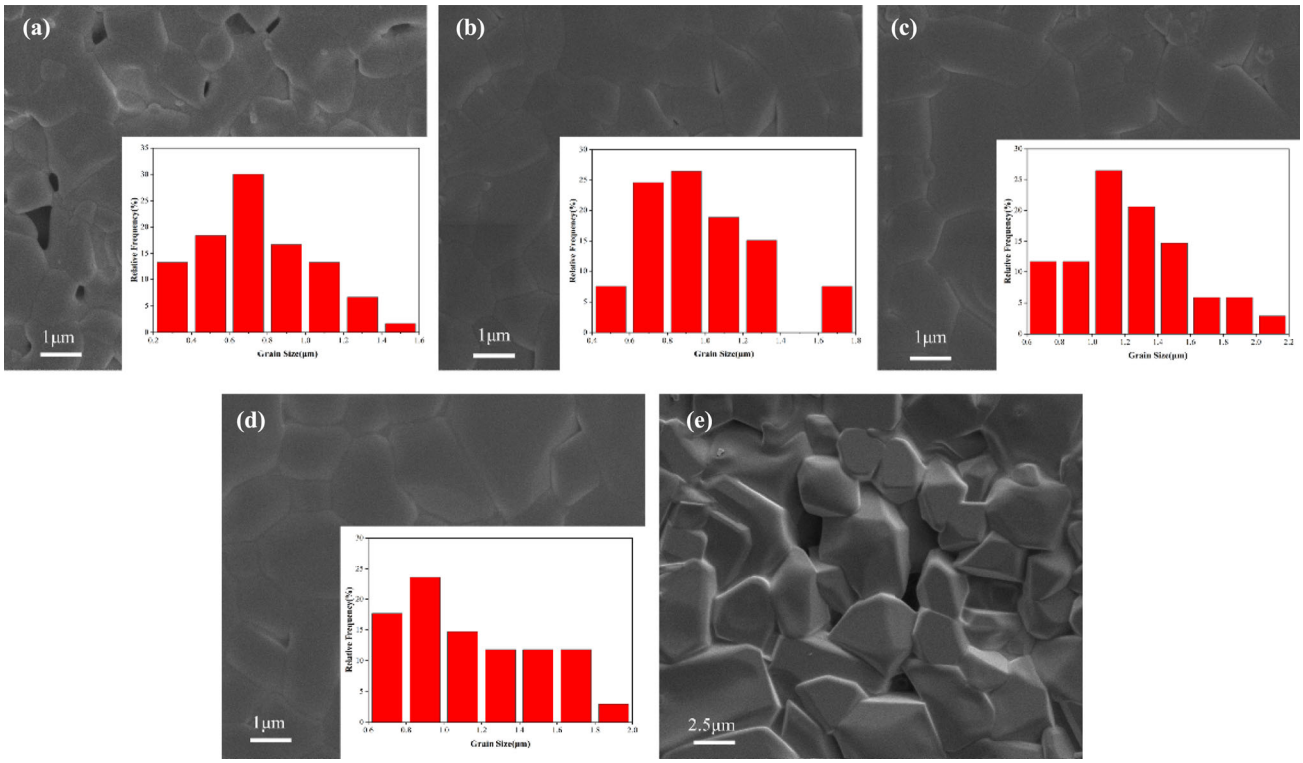

Fig. 4 Surface SEM graphs of $BiZn_2PO_6$ ceramics sintered at different temperatures. **a** 675 °C, **b** 700 °C, **c** 725 °C, **d** 750 °C, **e** 775 °C

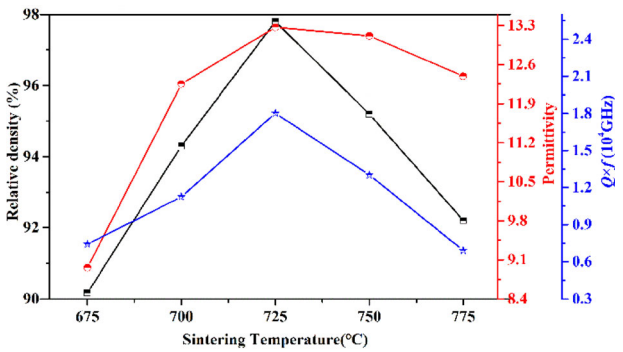

Fig. 5 The relative density, permittivity, and $Q \times f$ values of $BiZn_2PO_6$ ceramic sintered at different sintering temperatures

theoretical permittivity (ε_{theo}) of $BiZn_2PO_6$ ceramics by the following equation [35]:

$$\varepsilon_{theo} = \frac{3V_m + 8\pi\alpha_{theo}}{3V_m - 4\pi\alpha_{theo}} \tag{5}$$

The difference (Δ) between theoretical permittivity (ε_{theo}) and measured permittivity (ε_r) is defined as follows:

$$\Delta = \left| \frac{\varepsilon_{theo} - \varepsilon_r}{\varepsilon_r} \times 100\% \right| \tag{6}$$

Table 4 The minimum relative density and maximum relative density of microwave dielectric ceramics similar to $BiZn_2PO_6$

Materials	Minimum relative density (%)	Maximum relative density (%)
$BiZn_2PO_6$	90	97.8
$BiZn_2VO_6$	92	95.5
$BiCa_2VO_6$	91	95.6
$BiCu_2VO_6$	92.7	96.4
$BiMg_2VO_6$	93.8	98.1

The ε_{theo} of $BiZn_2PO_6$ in 725 °C is 13.165, and the deviation is 0.78% ($\leq$ 1%), indicating that ε_r is consistent with ε_{theo}. The permittivity in this work is closely related to ionic polarizability.

In addition, to explore the relationship between permittivity and relative density, the Bruggeman effective medium approximation theory can be introduced. It allows calculating the porosity-corrected permittivity (ε_{pc}) of $BiZn_2PO_6$ ceramics, as shown in Eq. (7) [36].

$$(1-f)\frac{\varepsilon_{theo}-\varepsilon_{pc}}{\varepsilon_{theo}+2\varepsilon_{pc}}+f\frac{\varepsilon_{air}-\varepsilon_{pc}}{\varepsilon_{air}+2\varepsilon_{pc}}=0 \quad (7)$$

In the above equation, ε_{air} represents the permittivity of air, and f represents the porosity of the sample. The results are listed in Table 5.

In summary, not only the ionic polarizability has an effect on the permittivity, but also the relative density or porosity is closely related to the permittivity, so the density of ceramics is an essential factor that must be considered. This conclusion also explains the tendency of the relative permittivity to decrease with decreasing relative density after exceeding the optimum sintering temperature. We could see that the quality factor of sintered samples increases when the sintering temperature increases from 675 to 725 °C. It was found that the density curves of the sintered samples reach the peak at 725 °C, and the $Q \times f$ value of $BiZn_2PO_6$ ceramic was 18,030 GHz at this time. The quality factor of $BiZn_2PO_6$ ceramics shows a gradually decreasing trend after reaching the maximum value, which is caused by the deterioration of the compactness of the samples due to over-firing. This rule coincides with the microscopic morphology changes reflected in the SEM micrographs in Fig. 4.

The $Q \times f$ value is affected by internal loss and external loss. The internal loss is mainly caused by the lattice vibration mode, while the external loss is caused by the second phase, oxygen vacancies, grain boundaries and the degree of densification or porosity [37, 38]. In this paper, since each sample presents a high relative density and all samples are pure phase ceramics, the primary influence on $Q \times f$ value is internal loss. Lattice energy is a measure of the binding force between ions, which is closely related to the internal loss, and can establish a relationship with the $Q \times f$ value. Therefore, the quality factor of microwave dielectric ceramics can be analyzed from the perspective of lattice energy. The total lattice energy of a complex crystal is the sum of the lattice energy of every single bond. The lattice energy of each chemical bond inside $BiZn_2PO_6$ ceramics could be obtained by the following formulas [39–42], and the calculated results are listed in Table 2. Among them, the different numbers in brackets in Table 2 represent different Walker positions of atoms in the crystal structure, as shown in Table 3. In addition, the number in the superscript is to distinguish chemical bonds of different lengths. For example, Bi-O(1)^1 and Bi-O(1)^2, where O(1)^1 and O(1)^2 represent Bi-O(1) bonds of different lengths.

$$U_{cal}=\sum_{\mu}U_b^{\mu} \quad (8)$$

$$U_b^{\mu}=U_{bc}^{\mu}+U_{bi}^{\mu} \quad (9)$$

$$U_{bc}^{\mu}=2100m\frac{(Z_+^{\mu})^{1.64}}{(d^{\mu})^{1.64}}f_c^{\mu} \quad (10)$$

$$U_{bi}^{\mu}=1270\frac{(m+n)Z_+^{\mu}Z_-^{\mu}}{d^{\mu}}\left(1-\frac{0.4}{d^{\mu}}\right)f_i^{\mu} \quad (11)$$

where U_{bc}^{μ} and U_{bi}^{μ} represented the covalent part and ionic part of the μ bond, respectively;Z_+^{μ} and Z_-^{μ} represented the valence states of cations and anions constituting the μ bond; m and n are the numbers of cations and anions in the μ bond and f_i^{μ} were the bond ionicity and bond covalency.

As can be seen from Table 2, the average lattice energy of the P–O bond is much higher than that of other types of chemical bonds, so the P–O bond contributes most of the lattice energy of $BiZn_2PO_6$ ceramics. The lattice energy is closely related to the $Q \times f$ value. The larger the lattice energy is, the higher the $Q \times f$ value is. Therefore, the $Q \times f$ value of the sample is significantly affected by the P–O bond.

Figure 6 displays the curve of the temperature coefficient of $BiZn_2PO_6$ ceramics changed with the sintering temperature. There is no visible law of τ_f values concerning sintering temperature in the figure, which means that the temperature coefficient varies

Table 5 α_{theo}, ε_{theo}, ε_r, ρ_{re}, ε_{pc} of $BiZn_2PO_6$ ceramics sintered at 725 °C

Sample	α_{theo}	ε_{theo}	ε_r	ρ_{re} (%)	ε_{pc}
$BiZn_2PO_6$	23.48	13.165	13.269	97.8	12.907

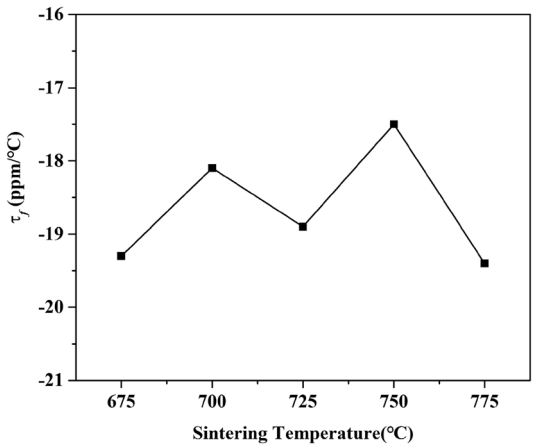

Fig. 6 The τ_f values of $BiZn_2PO_6$ sintered at different sintering temperatures

inconspicuously under this variable. At the optimal sintering temperature, the temperature coefficient of $BiZn_2PO_6$ ceramics is − 18.9 ppm/°C, which is an ideal value without adding other oxides to adjust.

4 Conclusions

The novel $BiZn_2PO_6$ ceramics were prepared by traditional solid-state reactions for microwave applications. The XRD spectrum showed that all sample peaks correspond to the standard card of pure $BiZn_2PO_6$ ceramic. The sintering performance, microstructure, relative density, and a series of microwave dielectric properties of $BiZn_2PO_6$ ceramics have been studied and demonstrated. The dielectric constant is related to ion polarizability and relative density. The $Q \times f$ value is related to density and lattice energy. According to the results of chemical bond decomposition and lattice energy calculation, the average lattice energy of the P-O bond is the largest, so it contributes the most to the $Q \times f$ value of $BiZn_2PO_6$ ceramics. In addition, the τ_f value of $BiZn_2PO_6$ ceramics is not sensitive to the sintering temperature. As expected, $BiZn_2PO_6$ exhibits excellent microwave dielectric properties at 725 °C for 4 h: ε_r = 13.269, $Q \times f$ = 18,030 GHz, τ_f = − 18.9 ppm/°C. $BiZn_2PO_6$ ceramics with excellent properties and compactness were obtained under ultra-low-temperature conditions, which is a possible candidate for ULTCC.

Acknowledgements

This work was supported by Major Projects of Science and Technology in Tianjin (Grant No. 18ZXJMTG00020).

Author contributions

PZ: Conceived and designed the work and revised the manuscript. XT: Performed the experiment, completed the data analyses and wrote the manuscript. MH: Helped perform the analysis with constructive discussions. SX: Approved the final version.

Data availability

All data generated or analyzed during this study are included in this article.

Code availability

Not applicable.

Declarations

Conflict of interest The authors declare that they have no known competing financial interests or personal relationships that could have appeared to influence the work reported in this paper.

Ethical approval Not applicable.

Consent to participate Written informed consent for participation was obtained from all participants.

Consent for publication Written informed consent for publication was obtained from all participants.

References

1. Y.H. Zhang, H.T. Wu, Crystal structure and microwave dielectric properties of La2(Zr1-xTix)(MoO4) 9(0 ≤ x ≤ 0.1) ceramics. J. Am. Ceram. Soc. **102**, 4092–4102 (2019)
2. L.X. Pang, D. Zhou, Modification of $NdNbO_4$ microwave dielectric ceramic by Bi substitutions. J. Am. Ceram. Soc. **102**, 2278–2282 (2019)

3. M.T. Sebastian, H. Jantunen, Low loss dielectric materials for LTCC applications: a review. Int. Mater. Rev. **53**, 57–90 (2008)
4. H. Zuo, X. Tang, H. Zhang, Y. Lai, Y. Jing, H. Su, Low-dielectric-constant $LiAlO_2$ ceramics combined with LBSCA glass for LTCC applications. Ceram. Int. **43**, 8951–8955 (2017)
5. Q. Lin, K. Song, B. Liu, H.B. Bafrooei, D. Zhou, W. Su, F. Shi, D. Wang, H. Lin, I.M. Reaney, Vibrational spectroscopy and microwave dielectric properties of $AY_2Si_3O_{10}$ (A = Sr, Ba) ceramics for 5G applications. Ceram. Int. **46**, 1171–1177 (2020)
6. B. Tang, S. Yu, H. Chen, S. Zhang, X. Zhou, Phase structure and microwave dielectric properties of Zr(Zn1/3Nb2/3)xTi2-xO6 ($0.2 \leq x \leq 0.8$) ceramics. J. Mater. Sci. Mater. Electron. **24**, 1475–1479 (2013)
7. T. Teranishi, R. Kanemoto, H. Hayashi, A. Kishimoto, Effect of the (Ba+Sr)/Ti ratio on the microwave-tunable properties of $Ba_{0.6}Sr_{0.4}TiO3$ ceramics. J. Am. Ceram. Soc. **100**, 1037–1043 (2017)
8. I.M. Reaney, D. Iddles, Microwave dielectric ceramics for resonators and filters in mobile phone networks. J. Am. Ceram. Soc. **89**, 2063–2072 (2006)
9. P. Zhang, L. Liu, M. Xiao, Y. Zhao, A novel temperature stable and high Q microwave dielectric ceramic in $Li_3(Mg_{1-x}Mn_x)_2NbO_6$ system. J. Mater. Sci. Mater. Electron. **28**, 12220–12225 (2017)
10. P. Zhang, L. Liu, M. Xiao, Microwave dielectric properties of high Q and temperature stable $Li_3(Mg_{1-x}Ni_x)_2NbO_6$ ceramics. J. Mater. Sci. Mater. Electron. **29**, 5057–5063 (2018)
11. M.T. Sebastian, R. Ubic, H. Jantunen, Low-loss dielectric ceramic materials and their properties. Int. Mater. Rev. **60**, 392–412 (2015)
12. H. Ohsato, T. Tsunooka, T. Sugiyama, K.-I. Kakimoto, H. Ogawa, S, Forsterite ceramics for millimeterwave dielectrics. J. Electroceramics. **17**, 445–450 (2006)
13. M.T. Sebastian, H. Wang, H. Jantunen, Low temperature co-fired ceramics with ultra-low sintering temperature: a review. Curr. Opin. Solid State Mater. Sci. **20**, 151–170 (2016)
14. H.T. Yu, J.S. Liu, W.L. Zhang, S.R. Zhang, Ultra-low sintering temperature ceramics for LTCC applications: a review. J. Mater. Sci. Mater. Electron. **26**(12), 9414–9423 (2015)
15. D. Thomas, P. Abhilash, M.T. Sebastian, Casting and characterization of $LiMgPO_4$ glass free LTCC tape for microwave applications. J. Eur. Ceram. Soc. **33**, 87–93 (2013)
16. P. Zhang, S. Wu, M. Xiao, The microwave dielectric properties and crystal structure of low temperature sintering $LiNiPO_4$ ceramics. J. Eur. Ceram. Soc. **38**, 4433–4439 (2018)
17. C.C. Xia, D.H. Jiang, G.H. Chen, Y. Luo, B. Li, C.L. Yuan, C.R. Zhou, Microwave dielectric ceramic of $LiZnPO_4$ for LTCC applications. J. Mater. Sci. Mater. Electron. **28**, 12026–12031 (2017)
18. R. Peng, Y. Li, G. Yu, Y. Lu, S. Li, Effect of Co^{2+} substitution on the microwave dielectric properties of $LiZnPO_4$ ceramics. J. Mater. Sci. Mater. Electron. **47**, 7281–7287 (2018)
19. R. Peng, Y. Lu, Z. Tao, D. Chen, L. Shi, Q. Zhang, Y. Li, Improved microwave dielectric properties and sintering behavior of $LiZnPO_4$ ceramic by Ni^{2+} doping based on first-principle calculation and experiment. Ceram. Int. **46**, 11021–11032 (2020)
20. R. Peng, Y. Li, H. Su, Y. Lu, L. Shi, Y. Yun, B. Liao, The modification of sintering and microwave dielectric properties of Mn^{2+} doped $LiZnPO_4$ ceramic. J. Mater. Sci. Technol. **9**, 4994–5006 (2020)
21. R. Nath, K.M. Ranjith, B. Roy, D.C. Johnston, Y. Furukawa, A.A. Tsirlin, Magnetic transitions in the spin-5/2 frustrated magnet $BiMn_2PO_6$ and strong lattice softening in $BiMn_2PO_6$ and $BiZn_2PO_6$ below 200 K. Phys. Rev. B. (2014). https://doi.org/10.1103/PhysRevB.90.024431
22. J. Chen, X. Zhang, S. Zhu, H. Ma, X. Li, H. Yu, F. Wang, Elastic anisotropy and thermodynamics properties of $BiCu_2PO_6$, $BiZn_2PO_6$ and $BiPb_2PO_6$ ceramics materials from first-principles calculations. Ceram. Int. **46**, 8575–8581 (2020)
23. D. Zhou, C.A. Randall, L.-X. Pang, H. Wang, J. Guo, G.-Q. Zhang, X.-G. Wu, L. Shui, X. Yao, Microwave dielectric properties of Li_2WO_4 ceramic with ultra-low sintering temperature. J. Am. Ceram. Soc. **94**, 348–350 (2011)
24. S.E. Kalathil, U.A. Neelakantan, R. Ratheesh, Microwave dielectric properties of ultralow-temperature cofirable $Ba_3V_4O_{13}$ ceramics. J. Am. Ceram. Soc. **97**, 1530–1533 (2014)
25. J. Honkamo, H. Jantunen, G. Subodh, M.T. Sebastian, P. Mohanan, Tape casting and dielectric properties of $Zn_2Te_3O_8$-based ceramics with an ultra-low sintering temperature. Int. J. Appl. Ceram. Technol. **6**, 531–536 (2009)
26. S.-F. Wang, Y.-F. Hsu, Y.-R. Wang, C.-C. Sung, Ultra-low-fire $Zn_2Te_3O_8$-$TiTe_3O_8$ ceramic composites. J. Am. Ceram. Soc. **94**, 812–816 (2011)
27. M.-Y. Chen, J. Juuti, C.-S. Hsi, C.-T. Chia, H. Jantunen, Dielectric properties of ultra-low sintering temperature Al_2O_3-BBSZ glass composite. J. Am. Ceram. Soc. **98**, 1133–1136 (2015)
28. H. Yu, K. Ju, K. Wang, A novel glass- ceramic with ultra- low sintering temperature for LTCC application. J. Am. Ceram. **97**, 704–707 (2014)
29. E. Ketatni, B. Mernari, F. Abraham, O. Mentre, Crystal structure of $BiZn_2PO6$. Filiation between related compounds. J. Solid State Chem. **153**, 48–54 (2000)
30. H. Luo, J. Li, J. Xu, L. Fang, Y. Tang, C. Li, A novel low-firing $BiZn_2VO_6$ microwave dielectric ceramic with low loss. J. Mater. Sci. Mater. Electron. **27**, 210–214 (2016)

31. H.-D. Xie, C. Chen, H.-H. Xi, R. Tian, X.-C. Wang, Synthesis, low temperature co-firing, and microwave dielectric properties of two ceramics BiM_2VO_6 (M = Cu, Ca). Ceram. Int. **42**, 989–995 (2016)
32. H.-D. Xie, H.-H. Xi, F. Li, C. Chen, Microwave dielectric properties of $BiMg_2VO_6$ ceramic with low sintering temperature. J. Inorg. Mater. **30**, 202–206 (2015)
33. H.L. Pan, L. Cheng, H.T. Wu, Relationships between crystal structure and microwave dielectric properties of Li2(Mg1-xCox)3TiO6 ($0 \leq x \leq 0.4$) ceramics. Ceram. Int. **43**, 15018–15026 (2017)
34. R.D. Shannon, G.R. Rossman, Dielectric constants of silicate garnets and the oxide additivity rule. Am. Mineral. **77**, 94–100 (1992)
35. R.D. Shannon, Dielectric polarizabilities of ions in oxides and fluorides. J. Appl. Phys. (1993). https://doi.org/10.1063/1.353856
36. D. Stroud, Stroud D, the effective medium approximations: some recent developments. Superlattice. Microst. **23**, 567–573 (1998). https://doi.org/10.1006/spmi.1997.0524
37. J. Li, L. Fang, H. Luo, J. Khaliq, Y. Tang, C. Li, Li_4WO_5: a temperature stable low-firing microwave dielectric ceramic with rock salt structure. J. Eur. Ceram. Soc. **36**, 243–246 (2016)
38. S.H. Yoon, D.-W. Kim, S.-Y. Cho, K.S. Hong, Investigation of the relations between structure and microwave dielectric properties of divalent metal tungstate compounds. J. Eur. Ceram. Soc. **26**, 2051–2054 (2006)
39. D.F. Xue, S.Y. Zhang, Calculation of the nonlinear optical coefficient of the $NdAl_3(BO_3)_4$crystal. J. Phys. Condens. Matter. **8**, 1949–1956 (1996)
40. Z.J. Wu, Q.B. Meng, S.Y. Zhang, Semiempirical study on the valences of Cu and bond covalency in $Y_{1-x}Ca_xBa_2Cu_3O_{6+y}$. Phys. Rev. B. **58**, 958–962 (1998)
41. Q.B. Meng, Z.J. Wu, S.Y. Zhang, Evaluation of the energy barrier distribution in many-particle systems using the path integral approach. J. Phys. Condens. Matter. **10**, 85–88 (1998)
42. P. Zhang, Y. Zhao, L. Li, The correlations among bond ionicity, lattice energy and microwave dielectric properties of (Nd1−xLax)NbO4 ceramics. Phys. Chem. Chem. Phys. **17**, 16692–16698 (2015)